Stem Cell Reports
Article

ISSCR

OPEN ACCESS

Loss of endosomal exchanger NHE6 leads to pathological changes in tau in human neurons

Marty A. Fernandez,[1] Fatmata Bah,[1] Li Ma,[2,3] YouJin Lee,[2,3] Michael Schmidt,[2,3] Elizabeth Welch,[1] Eric M. Morrow,[2,3,4,*] and Tracy L. Young-Pearse[1,*]

[1]Ann Romney Center for Neurologic Diseases, Brigham and Women's Hospital and Harvard Medical School, Boston, MA 02115, USA
[2]Department of Molecular Biology, Cell Biology and Biochemistry, Brown University, Providence, RI 02912, USA
[3]Center for Translational Neuroscience, Carney Institute for Brain Science and Brown Institute for Translational Science (BITS), Brown University, Providence, RI 02912, USA
[4]Department of Psychiatry and Human Behavior, Warren Alpert Medical School of Brown University, Providence, RI 02912, USA
*Correspondence: eric_morrow@brown.edu (E.M.M.), tpearse@bwh.harvard.edu (T.L.Y.-P.)
https://doi.org/10.1016/j.stemcr.2022.08.001

SUMMARY

Disruption of endolysosomal and autophagy-lysosomal systems is increasingly implicated in neurodegeneration. Sodium-proton exchanger 6 (NHE6) contributes to the maintenance of proper endosomal pH, and loss-of function mutations in the X-linked NHE6 lead to Christianson syndrome (CS) in males. Neurodegenerative features of CS are increasingly recognized, with postmortem and clinical data implicating a role for tau. We generated cortical neurons from NHE6 knockout (KO) and isogenic wild-type control human induced pluripotent stem cells. We report elevated phosphorylated and sarkosyl-insoluble tau in NHE6 KO neurons. We demonstrate that NHE6 KO leads to lysosomal and autophagy dysfunction involving reduced lysosomal number and protease activity, diminished autophagic flux, and p62 accumulation. Finally, we show that treatment with trehalose or rapamycin, two enhancers of autophagy-lysosomal function, each partially rescue this tau phenotype. We provide insight into the neurodegenerative processes underlying NHE6 loss of function and into the broader role of the endosome-lysosome-autophagy network in neurodegeneration.

INTRODUCTION

Dysfunction of the endolysosomal and autophagy-lysosomal systems is a critical molecular player in neurologic disease. Neurons are particularly vulnerable to dysfunction of these pathways and consequent sorting and clearance defects due to their postmitotic state, longevity, and highly specialized morphology engendering specific trafficking requirements (Giovedi et al., 2020; Malik et al., 2019). Lysosomal deficiencies have long been known to have neurodevelopmental impacts and are associated with over 50 lysosomal storage disorders that profoundly affect the CNS (Parenti et al., 2021). In addition, a central role for endolysosomal and autophagy defects is increasingly appreciated in many neurodegenerative disorders, with defects in sorting and degradation leading to progressive neuronal dysfunction and accumulation of neurotoxic proteins (Colacurcio et al., 2018; Nixon et al., 2008; Van Acker et al., 2019).

A key feature of the maturation of early endosomes to late endosomes to lysosomes is the progressive acidification of these cellular compartments (Casey et al., 2010). Tight control of luminal pH is crucial for regulating many aspects of endolysosomal function such as binding and dissociation of receptors and ligands for proper trafficking and recycling (Borden et al., 1990; Dautry-Varsat et al., 1983; Yamashiro and Maxfield, 1984), activity and degradative capacity of lysosomal hydrolases and other enzymes en route through the pathway (Casey et al., 2010; Pillay et al., 2002), and signaling from molecules within endosomes (Diering and Numata, 2014; Ouyang et al., 2013). Proper pH of the endosomal lumen and maturation to lysosomes is regulated by the opposing actions of pumps and exchangers: the vacuolar-type ATPase pumps protons into the endosome in an ATP-dependent manner, while sodium-proton exchangers (NHEs, with NHE6 and 9 localizing to endosomes) allow for the leak of luminal protons out of the endosome in exchange for cations (Casey et al., 2010; Donowitz et al., 2013; Kondapalli et al., 2014; Mellman, 1992).

Loss of NHE6 activity has profound neurologic consequences. The gene encoding NHE6 is located on the X chromosome (SLC9A6), and loss-of-function mutations in NHE6 in males cause the neurologic disorder Christianson syndrome (CS). Affected males present with a severe neurodevelopmental syndrome characterized by intellectual disability, autistic behaviors, nonverbal status, and postnatal microcephaly (Christianson et al., 1999; Gilfillan et al., 2008; Pescosolido et al., 2014). The cellular consequences of NHE6 loss of function have been studied in NHE6-null mouse models. Neurons from these CS mice exhibit endosomal hyperacidification, a consequence of loss of proton leak from the endosome, as well as impoverished neuronal arborization and attendant circuit dysfunction (Ouyang et al., 2013). NHE6-null mouse neurons also show defects in endosomal maturation and trafficking, which results in enhanced exosome secretion, decreased endosome-lysosome fusion, and lysosome deficiency (Pescosolido et al., 2021).

In addition to its clear neurodevelopmental impacts, neurodegenerative features of NHE6 loss of function are increasingly appreciated. NHE6-null mice and rats exhibit progressive Purkinje cell loss, cortical thinning, and gliosis (Lee et al., 2021; Sikora et al., 2016; Stromme et al., 2011; Xu et al., 2017). NHE6-null rats show deposition of Aβ and tau, as well as neuronal degeneration (Lee et al., 2021). In addition, a study of postmortem brain tissue reported extensive cortical and subcortical tau deposition in two CS patient brains (Garbern et al., 2010). Moreover, heterozygous females in CS pedigrees have been diagnosed clinically with neurodegenerative diseases associated with tau deposition, such as progressive supranuclear palsy, corticobasal degeneration, and atypical parkinsonism (Pescosolido et al., 2019; Sinajon et al., 2016). Additionally, decreased NHE6 expression in postmortem brain correlates with increased tau deposition in the Religious Orders Study/Memory and Aging Project (ROS/MAP) cohorts (Pescosolido et al., 2019). Reduced NHE6 expression also has been reported in Alzheimer disease (AD) brains (Prasad and Rao, 2015).

We hypothesized that loss of NHE6 causes endolysosomal dysfunction and changes in tau protein relevant to AD and related disorders (ADRDs) in human neurons. We generated cortical neurons from NHE6-null and isogenic wild-type (WT) control human induced pluripotent stem cell (iPSC) lines (Lizarraga et al., 2021). We report elevated levels of phosphorylated and insoluble tau in NHE6 knockout (KO) neurons, along with changes in endosome and lysosome size and area, reduced lysosomal protease activity, and reduced autophagic function. Importantly, the elevated phospho-tau phenotype was partially rescued by treatment with trehalose or rapamycin, two enhancers of autophagy-lysosomal function, suggesting that the tau defects in NHE6 KO neurons are secondary to dysfunction of the autophagy-lysosomal system. This study provides insight into the connections between endolysosomal defects and the etiology of tauopathies and further elucidates key opportunities for therapeutic intervention.

RESULTS

Generation and differentiation of isogenic WT and NHE6 KO iPSC lines

Isogenic WT and NHE6 KO monoclonal lines described in Figure 1A were generated using CRISPR-Cas9 gene editing. The generation and characterization of these lines has been previously described (Lizarraga et al., 2021). KO of NHE6 was confirmed by immunoprecipitation (IP) and western blot (WB) of NHE6 in iPSC lysates (Figure 1B). As has been previously reported, IP of NHE6 prior to WB is necessary to mitigate antibody cross-reactivity with other NHE proteins (Lizarraga et al., 2021).

NHE6 KO and WT iPSC lines were differentiated into induced layer 2/3 cortical neurons (iNs) via the expression of NGN2 (Lagomarsino et al., 2021; Srikanth et al., 2018; Zhang et al., 2013). WT and KO lines were plated and differentiated in parallel for 21 days, at which point they express synaptic markers and exhibit electrophysiological activity (Lagomarsino et al., 2021; Srikanth et al., 2018; Zhang et al., 2013). Immunostaining for the neuronal proteins Tau, NeuN, and βIII-tubulin demonstrated equivalent neuronal differentiation efficiency across lines (Figure 1C). RNA sequencing revealed that NHE6 is most highly expressed in iNs when compared with iPSC-derived astrocytes and microglia (Figure S1). As shown in Figure S1, we did not observe significant differences in cell death between WT and KO iNs as assessed by terminal deoxynucleotidyl transferase dUTP nick end labeling staining.

Loss of NHE6 leads to ADRD-related changes in tau protein in human iPSC-derived neurons

To elucidate the effects of NHE6 loss of function on tau, we examined whether NHE6 KO results in pathological changes in tau protein in human iPSC-derived neurons. We performed sequential protein extractions from the neurons to obtain TBS-soluble, 1% sarkosyl-soluble, and 1% sarkosyl-insoluble fractions, as shown in Figure S2A. Next, we examined the levels of total and phosphorylated tau in each fraction by WB with K9JA (Dako), an antibody that recognizes the C-terminal half of tau, and AT8 (Invitrogen), which recognizes tau phosphorylated at Ser202 and Thr205 (Figure 2A). Phosphorylation at this epitope has been proposed to be one of the earliest phosphorylation events in AD pathogenesis (Biernat et al., 1992; Braak et al., 1994), and we have observed elevation of phosphorylation at these sites in fAD neurons (Muratore et al., 2017). Both NHE6 KO clones showed a roughly 1.5-fold increase in the ratio of p202 and p205 tau to total tau compared with the isogenic WT control line in all three fractions across independent differentiations (Figure 2B). We next analyzed levels of tau and phospho-tau relative to total protein in each fraction. In the absence of a known loading control present equally in these different cellular fractions, we utilized Revert total protein staining (Licor) to normalize for protein loading (Figure 2A). We found increased levels of total tau relative to total protein in the sarkosyl-insoluble fraction in NHE6 KO neurons compared with WT neurons (Figures 2C and S2B). p202,205 tau was elevated relative to total protein in all fractions to a similar degree (Figures 2D and 2E).

We next examined additional phospho-tau epitopes. We found that phosphorylation at Thr181 relative to total tau and Ser404 relative to total protein were elevated in both NHE6 KO clones compared with WT in the TBS-soluble fraction (Figure 3). Individual clones also exhibited

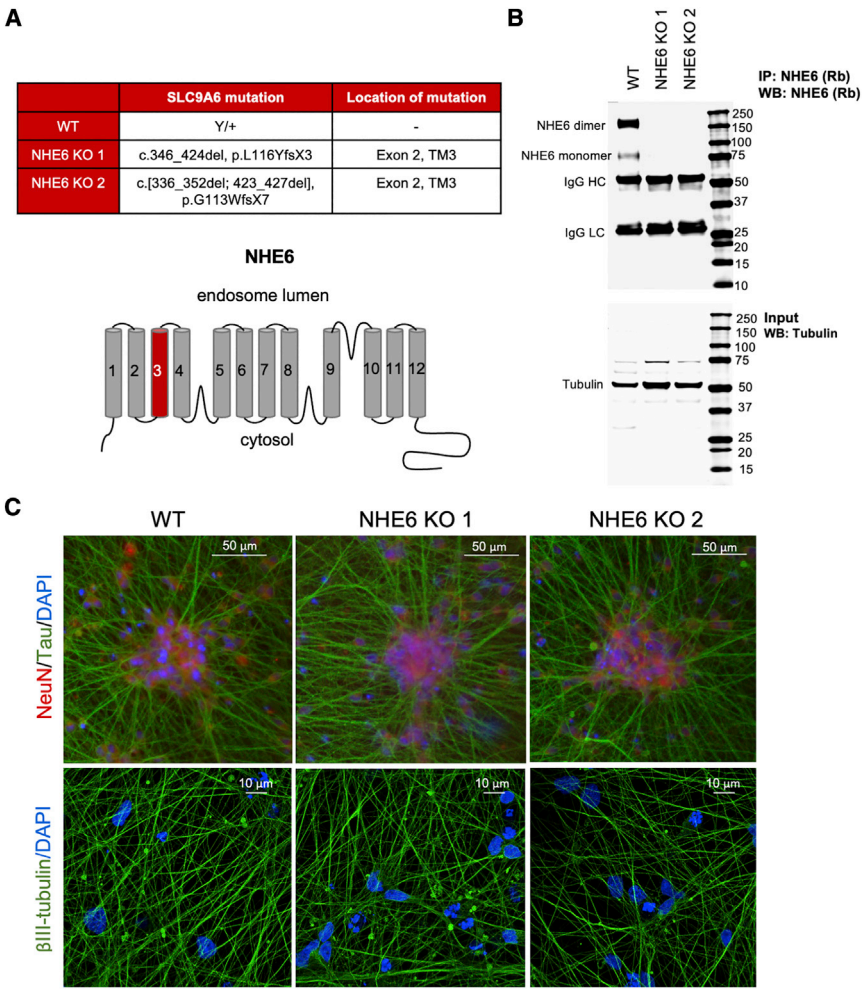

Figure 1. Characterization of WT and NHE6 knockout (KO) isogenic lines

(A) A summary of the genome editing information that generated the isogenic NHE6 KO iPSC lines. A schematic of the NHE6 protein is shown to indicate the location of transmembrane (TM) domains. TM3, the domain targeted by CRISPR and location of the frameshift mutations in the KO lines, is highlighted in red.

(B) Loss of NHE6 protein in KO iPSC lines was confirmed by WB following NHE6 immunoprecipitation.

(C) Control and NHE6 KO iPSC lines were differentiated into cortical layer 2/3 excitatory neurons using the NGN2-induced neuron (iN) protocol. Representative images of immunostaining of fixed day 21 neurons for neuronal markers tau, NeuN, and βIII-tubulin relay equivalent differentiation of the isogenic lines to a neuronal fate.

elevated levels of phosphorylation at these epitopes in the 1% sarkosyl-soluble fraction (Figures 3D, S2C, and S2D).

iN differentiations described in our previous work (Lagomarsino et al., 2021; Muratore et al., 2017; Srikanth et al., 2018) and in other published studies (Zhang et al., 2013) are carried out with BDNF, GDNF, and CNTF in the culture media to promote neuronal growth and survival in culture. However, the neurodevelopmental phenotype of reduced neuronal arborization observed in NHE6 KO primary mouse neurons is mediated by attenuated endosomal BDNF/TrkB signaling; this signaling deficit and impoverished neurite phenotype could be rescued by the addition of exogenous BDNF (Ouyang et al., 2013). Because of these findings, the experiments described above were carried out without the addition of these growth factors. To determine whether culturing neurons with these growth factors affects the elevated phospho-tau phenotype we observed in the KO lines, we performed an additional set of experiments in the presence of BDNF, GDNF, and CNTF. As shown in Figure S3, we found that culture of the iNs with growth factors using the standard NGN2 protocol diminished the elevation of p202,205 tau in the KO lines. Under these culture conditions, we still observed a significant elevation of p202,205 tau relative to total tau in both KO clones, but only in the 1% sarkosyl-insoluble fraction. We conclude that the effect on tau was still present, but dampened, by supplement of media with growth factors.

To understand the specificity of the observed effects of loss of NHE6 on tau protein, we examined these neurons for biochemical changes in another aggregation-prone and disease-associated protein, α-synuclein, in 1% sarkosyl-soluble iN extracts by WB (Figure S4). We identified an α-synuclein monomer of 14 kDa and an apparent dimer of ~30 kDa. As shown in Figure S4B, levels of α-synuclein monomer and dimer were not altered in NHE6 KO iNs compared to WT iNs. This suggests that NHE6 KO does not induce the accumulation of a second aggregation-prone protein in iNs.

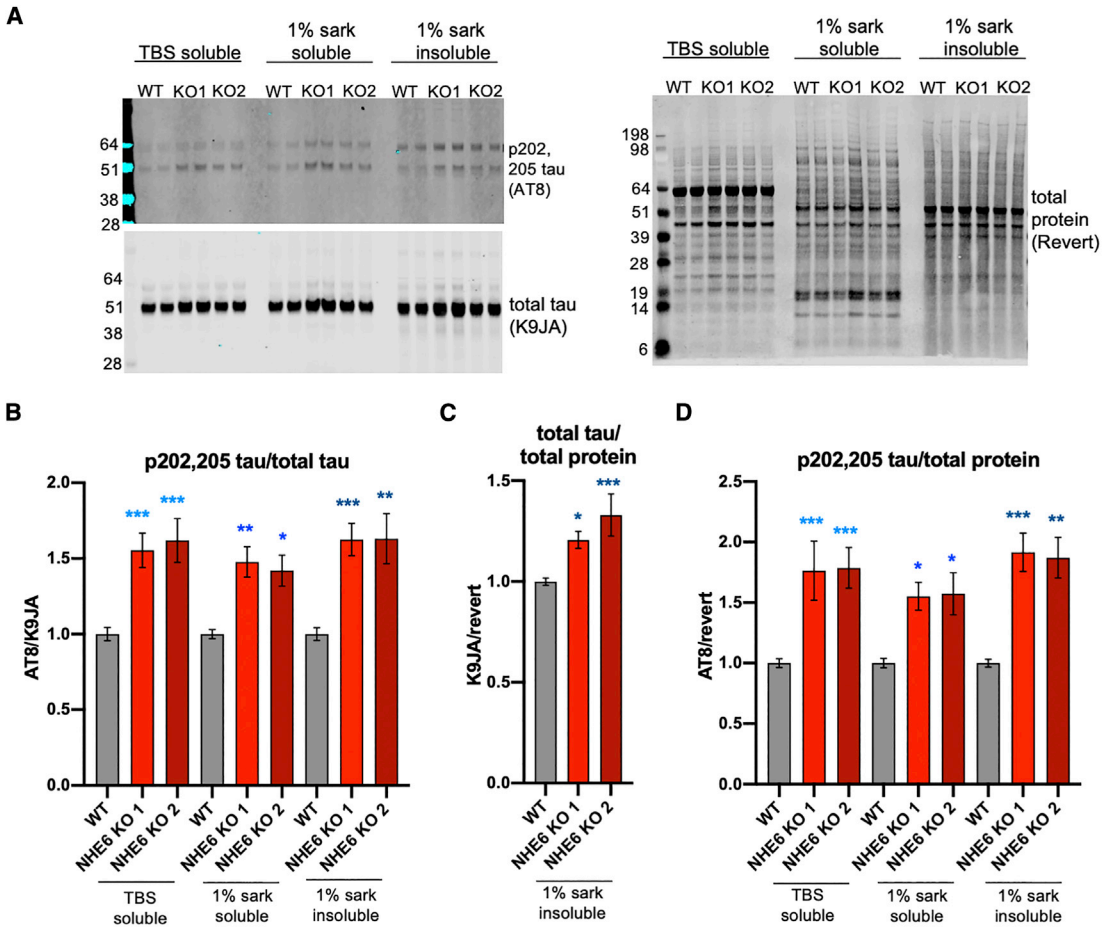

E

	TBS soluble		1% sarkosyl soluble		1% sarkosyl insoluble	
	KO 1	KO 2	KO 1	KO 2	KO 1	KO 2
p202,205 tau/total tau	***	***	**	*	***	**
p202,205 tau/total protein	***	***	*	*	***	**
total tau/total protein	ns	ns	ns	ns	*	***

Figure 2. NHE6 KO results in elevated phosphorylated tau and sarkosyl-insoluble tau in human iPSC-derived neurons

iNs were differentiated for 21 days. On day 21, TBS-soluble, 1% sarkosyl-soluble, and 1% sarkosyl-insoluble extracts were prepared sequentially, and levels of total tau and phosphorylated tau examined by WB.

(A) Tau phosphorylated at Ser202/Thr205 was examined by WB using the antibody AT8 (Invitrogen), and total tau was detected using the antibody K9JA (DAKO). Revert total protein stain (Licor) was used to normalize for protein loading across fractions to examine changes in tau solubility.

(B) Quantification of p202,205 tau levels relative to total tau levels measured by WB from four independent differentiations, two wells per line per differentiation.

(C) Levels of total tau in the 1% sarkosyl-insoluble fraction were quantified across four independent differentiations, two wells per line per differentiation, and found to be elevated relative to total protein (measured by revert staining) in the 1% sarkosyl-insoluble fraction.

(D) The levels of p202,205 tau were quantified and normalized to total protein (as measured by revert staining) across four independent differentiations, two wells per differentiation.

(E) A table summarizing the changes in p202,205 tau and total tau in NHE6 KO lines compared with WT in TBS, 1% sarkosyl-soluble, and 1% sarkosyl-insoluble fractions. For all graphs, mean ± SEM, *$p < 0.05$, **$p < 0.01$, ***$p < 0.005$, ns = no significance by one-way ANOVA and Sidak's post test comparing KO to WT within each fraction.

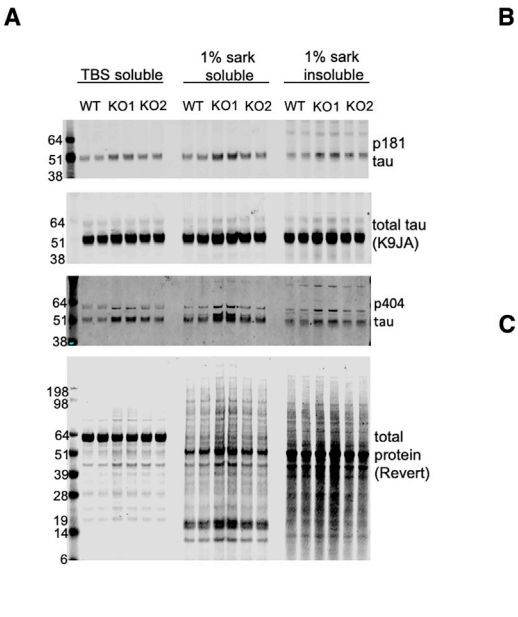

Figure 3. NHE6 KO results in elevated phosphorylated Thr181 and Ser404 tau in the TBS-soluble fraction

(A) Tau phosphorylated at Thr181 and Ser404 was examined by WB along with total tau (K9JA) and revert staining for normalization.

(B and C) Quantification of TBS-soluble p181 tau relative to total tau across four independent differentiations, two wells per differentiation (B), and p404 tau relative to total protein across three independent differentiations, two wells per differentiation (C).

(D) A table summarizing the changes in p181 and p404 tau in NHE6 KO lines compared with WT in TBS, 1% sarkosyl-soluble, and 1% sarkosyl-insoluble fractions. For all graphs, mean ± SEM, *p < 0.05, **p < 0.01, ****p < 0.001, ns = no significance by one-way ANOVA and Sidak's post test comparing WT to KO within each fraction.

D

	TBS soluble		1% sarkosyl soluble		1% sarkosyl insoluble	
	KO 1	KO 2	KO 1	KO 2	KO 1	KO 2
p181 tau/total tau	**	*	ns	ns	*	ns
p404 tau/total protein	****	*	*	ns	ns	ns

A CS-causing mutation in NHE6 also leads to increased tau phosphorylation

We generated iNs from an iPSC line obtained from a CS patient alongside two CRISPR-corrected isogenic control clones (Ma et al., 2021). The mutation, occurring in exon 12 (predicted TMD12) of the NHE6 protein (Figure 4A), leads to a premature stop codon and loss of NHE6 protein (Figure 4B) (Ma et al., 2021). We examined levels of p202,205 and total tau in RIPA-soluble lysates (Figure 4C) and found that CS neurons exhibited an increased ratio of phospho-tau relative to total tau compared with the corrected isogenic WT controls (Figure 4D).

NHE6 KO leads to subtle increases in amyloid precursor protein processing by β-secretase but does not significantly alter Aβ levels

The membrane-spanning amyloid precursor protein (APP) undergoes sequential proteolysis by β- and γ-secretases to generate Aβ, which has been implicated in the pathogenesis of AD (De Strooper et al., 2012; Haass and Selkoe, 1993; Hampel et al., 2021). The membrane-anchored β-secretase is active in the mildly acidic environment of the early endosome, so APP processing by β-secretase occurs within the early endosome following endocytosis of APP (Das et al., 2013; Sannerud et al., 2011; Schneider et al., 2008; Vassar et al., 2009). This cleavage releases the soluble ectodomain of APP (APPsβ) and leaves a remaining C-terminal stub, CTFβ, within the membrane; CTFβ then undergoes intramembrane cleavage by γ-secretase to liberate Aβ into the endosomal lumen (Esler and Wolfe, 2001). Alternatively, APP can be cleaved at the plasma membrane by α-secretase, which releases APPsα and precludes Aβ generation. The proteolytic processing of APP is illustrated in Figure 5A.

It has been reported in non-neuronal cell lines that the hyperacidic endosomal pH caused by experimentally induced knockdown of NHE6 leads to increased β-secretase activity and elevated Aβ production (Prasad and Rao, 2015). Additionally, we and others have shown that changes in Aβ production caused by familial AD (fAD) mutations in APP can lead to increased tau phosphorylation in human iPSC-derived neurons (Israel et al., 2012; Muratore et al., 2014) and that late-onset AD iNs can generate an elevation of long to short Aβ peptides and a change in tau oligomerization (Lagomarsino et al., 2021). For these reasons, we interrogated whether NHE6 loss of function leads to changes in Aβ production that could potentially contribute to the tau phenotype we observed.

First, we examined levels of full-length APP and APP CTFs present in WT and NHE6 KO iNs by WB, and we found no

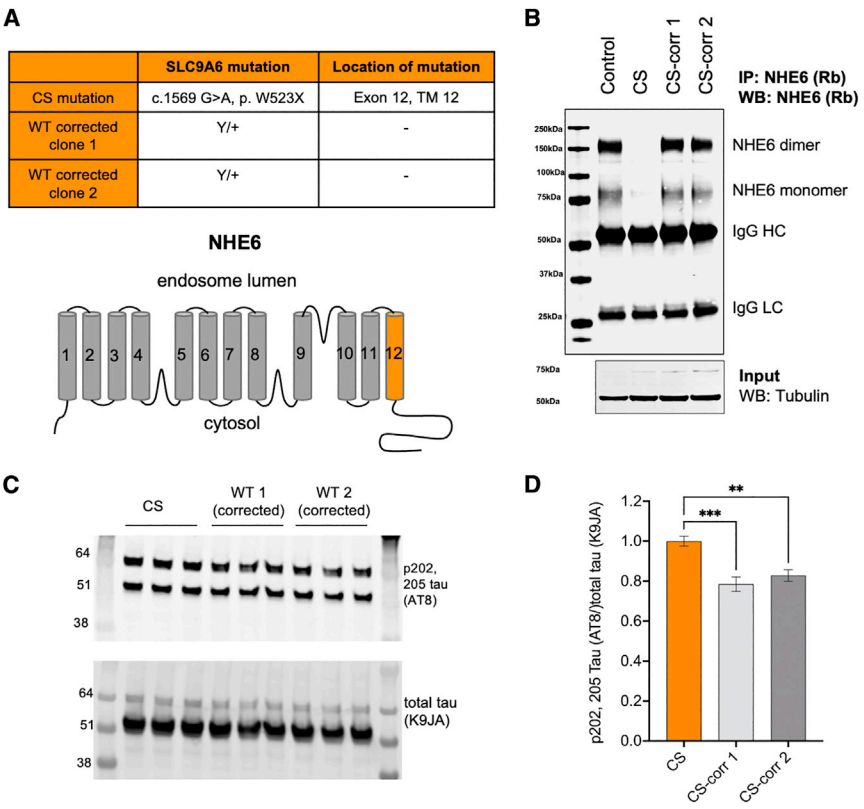

Figure 4. A CS mutation in NHE6 results in elevated phosphorylated tau levels in human iPSC-derived neurons

(A) An iPSC line was generated from a male CS patient and harbors an NHE6 loss function mutation in transmembrane domain 12 (highlighted in orange). Two CRISPR-corrected WT isogenic control lines were generated.

(B) Loss of NHE6 protein in the CS iPSC line was confirmed by WB following NHE6 immunoprecipitation.

(C) p202, 205 tau, and total tau were examined by WB.

(D) Quantification of WB data from three independent differentiations, two wells per differentiation for CS line and both WT clones. Mean ± SEM, **p < 0.01 ***p < 0.005 by one-way ANOVA followed by Dunnett's post test, comparing to the parental CS line.

differences in the levels in these neurons (Figures 5B and 5C). Next, conditioned media were collected from iNs on d21 and levels of APPsα and APPsβ in the media measured by ELISA to quantify β- versus α-secretase cleavage of APP (Figures 5D–5F). We found a slight but significant elevation in the ratio of APPsβ versus APPsα (Figure 5D), suggesting an increase in the level of APP processing by β-secretase compared with α-secretase. We found that this elevation in APPsβ/APPsα occurred even when we cultured the cells with exogenous growth factors, suggesting that APP processing and secretase activities were not affected by these culture conditions (Figure S5A). There is some variability across clones in the amounts of APPsα and APPsβ when normalized to total protein in the lysates. This may be explained by clonal variation but more likely is due to the less sensitive method of normalizing to total protein concentration of lysates compared with the more robust measurement of the ratio of secreted APPsα and APPsβ.

We then measured levels of Aβ 37, 38, 40, and 42 in the conditioned media. We did not observe a change in the levels (Figures 5G–5J), nor the ratios of Aβ peptides released in the media (Figures 5K–5M). Last, we did not observe a change in the levels of Aβ present in iN lysates (which includes both intracellular and cell-associated Aβ) (Figures 5N–5P). This same result was observed in iNs cultured without growth factors (Figures S5B–S5F). To summarize, the apparent subtle increase in APP processing by β-secretase that we observed with NHE6 KO did not ultimately result in a detectable elevation in Aβ levels; therefore, we conclude that increased Aβ levels or alterations in Aβ ratios are not the cause of the elevated phospho-tau phenotype we observed in NHE6 KO iNs.

NHE6 KO leads to lysosomal and autophagy dysfunction in iNs

Previous studies in NHE6-null mice and rats reported abnormal accumulation of GM2 ganglioside and unesterified cholesterol within late endosomes and lysosomes of neurons and reduced neuronal β-hexosaminidase activity (Lee et al., 2021; Sikora et al., 2016; Stromme et al., 2011); these phenotypes are typical of lysosomal storage disorders and suggest compromised lysosomal function in NHE6 KO neurons. In addition, we recently found that NHE6-null mouse neurons display defects in endosome maturation and endosome-lysosome fusion, which contribute to deficiencies in lysosome function (Pescosolido et al., 2021). Therefore, here we examined human NHE6 KO neurons for endosomal and lysosomal defects. We first used high-content image analysis to quantify the number and area of early endosomes per cell by immunostaining fixed neurons for the early endosome marker EEA1. Representative

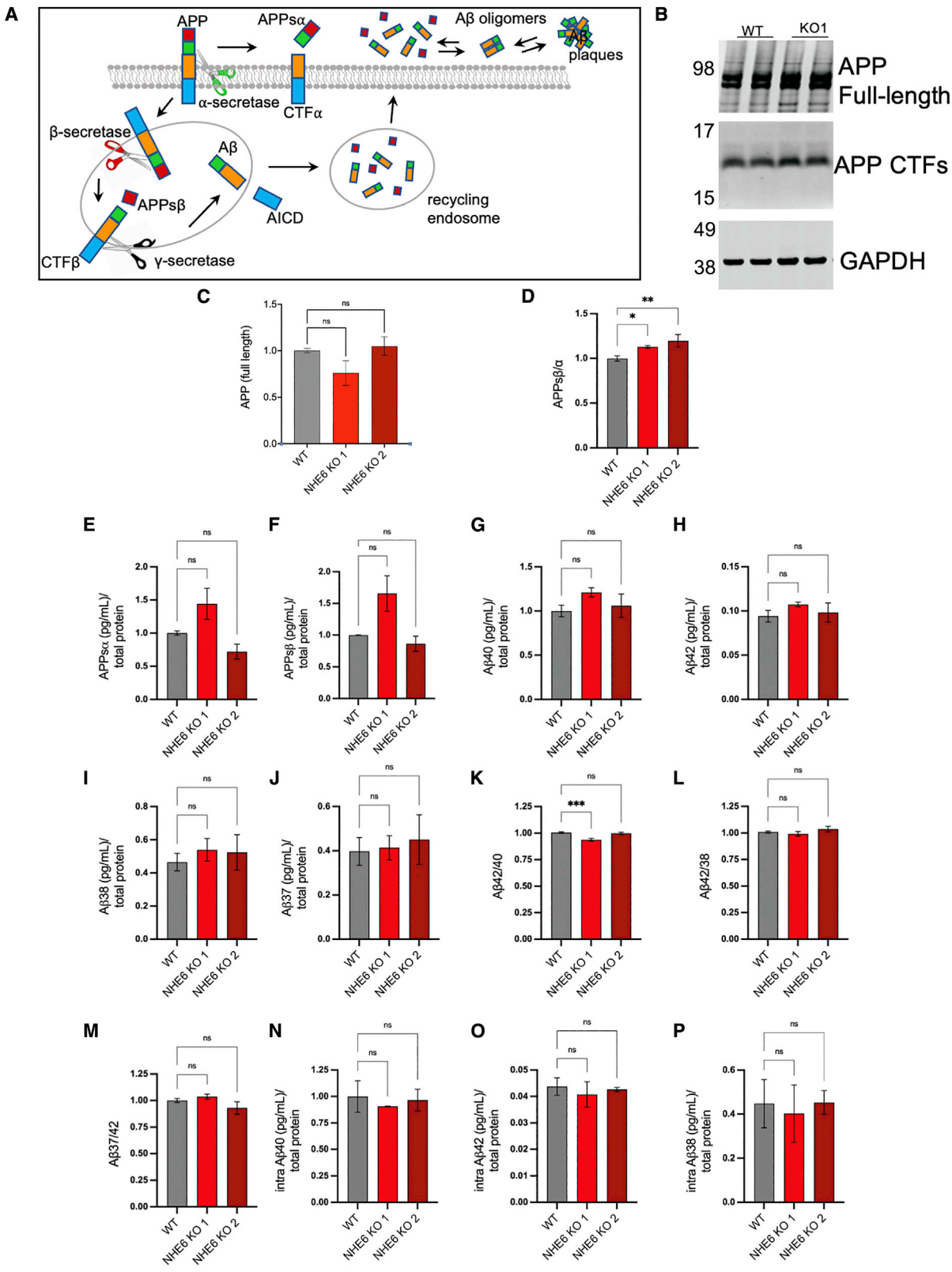

(legend on next page)

immunostaining images of endosomes in WT and KO iNs are shown in Figures 6A and 6B. Cells were imaged using an IN Cell analyzer, and EEA1-positive puncta within the cell soma were identified, assigned to cells, counted, and quantified using Cell Profiler. We found that the number of EEA1-labeled puncta present in the soma per cell was increased with NHE6 KO (Figure 6C). In addition, the average area of EEA1 puncta was decreased in the NHE6 KO lines (Figure 6D). In contrast, the area of RAB7+ late endosomes was increased (Figures 6E and 6F). To examine lysosomes, we used two methods: LysoTracker dye (Thermo Fisher Scientific) or LAMP1 immunostaining (Figures 6E and 6G–6I). We found that, compared with WT, NHE6 KO iNs had reduced numbers of lysotracker-positive puncta in the soma per cell (Figure 6H), while the average puncta area (per puncta) was unchanged (Figures 6G and 6I). Of note, LysoTracker labels lysosomes based upon their acidic pH. Therefore, hyperacidified late endosomes also may be labeled with this dye. Nonetheless, numbers of LysoTracker puncta were reduced with NHE6 KO. These changes in endosomal and lysosomal number and morphology led to us to investigate whether functional changes in lysosomal activity were present in the NHE6 KO neurons. We quantified lysosomal protease activity using a fluorescent cathepsin B activity assay, and as shown in Figure 6J, NHE6 KO iNs exhibited a reduction in cathepsin B activity compared with WT neurons.

Because degradation of intracellular materials via autophagy requires proper lysosomal function for clearance of cargo, we examined whether NHE6 KO neurons also exhibit defects in autophagy. We first measured the levels of autophagy-specific substrate p62 in the NHE6 KO and WT neurons by WB, as p62 accumulation is indicative of autophagy dysfunction in cells. As shown in Figures 6K and 6L, p62 was significantly elevated in NHE6 KO iNs compared with WT cells. We next measured autophagic flux. Autophagic flux is a measure of the dynamic process of autophagosome formation and turnover by the lysosome; decreased flux indicates dysfunction of this pathway. We treated neurons with either bafilomycin A or chloroquine (alongside vehicle controls) to block the fusion of the autophagosome with the lysosome. We then lysed these neurons, performed LC3 WBs to quantify the levels of autophagosome-associated LC3-II in the treated versus untreated neurons, and used this data to calculate autophagic flux (flux = (LC3-II/GAPDH with bafilomycin or chloroquine treatment) – (LC3-II/GAPDH with vehicle treatment)) (Figures 6M–6O). We found that NHE6 KO iNs exhibited reduced autophagic flux compared with WT iNs in both the bafilomycin A and chloroquine experimental paradigms (Figures 6N and 6O).

Elevated phospho-tau in NHE6 KO neurons is partially rescued by treatment with trehalose or rapamycin, two enhancers of autophagy

The evidence of endolysosomal and autophagy-lysosomal defects in NHE6 KO iNs described above led us to hypothesize that the elevated phospho-tau phenotype in these neurons is secondary to autophagy-lysosomal dysfunction. To probe this further, we tested whether treatment of NHE6 KO neurons with trehalose could correct this tau phenotype. Trehalose is a non-reducing disaccharide that has been proposed to enhance autophagy in an mTor-independent manner (Belzile et al., 2016; Castillo et al., 2013; Klionsky et al., 2016; Sarkar et al., 2007; Zhang et al., 2014). Trehalose has been studied for many years in numerous disease models and has been shown to enhance the degradation of a range of neurotoxic proteins, such as mutant TDP43, mutant SOD1, and tau (Casarejos et al., 2011; Castillo et al., 2013; Kruger et al., 2012; Rodriguez-Navarro et al., 2010; Sarkar et al., 2007; Wang et al., 2018). We treated WT and KO neurons with trehalose beginning on d17 and analyzed the levels of p202,205 tau and total tau in RIPA-extracted lysates by WB at d22 (Figure 7A). As shown in Figure 7B, we found that KO iNs displayed the expected elevated ratio of p202,205 tau relative to total tau, and that this phenotype was partially rescued by treatment with trehalose. Notably, trehalose did not alter the phospho-tau to total tau ratio in WT iNs, indicating that trehalose treatment did not cause a general

Figure 5. NHE6 KO does not affect secreted or intracellular Aβ levels in iNs

(A) A schematic of APP processing by α, β, and γ secretases at the cell surface and within the early endosome.

(B and C) WB analysis of APP levels in WT and NHE6 KO iN. (C) is a quantification of full-length APP levels normalized to GAPDH from four independent differentiations.

(D–F) APPsβ and APPsα levels in the conditioned media of day 21 iNs were measured by ELISA and normalized to total protein as measured by bicinchoninic acid assay of protein lysates obtained from the cells within the wells.

(G–J) Aβ 40, 42, 38, and 37 levels in the conditioned media of day 21 iNs were measured via ELISA. Data were normalized to total protein as in (B) and (C).

(K–M) Ratios of Aβs measured in (C)–(F).

(N–P) Levels of intracellular (and cell-associated) Aβs were measured in iN lysates and normalized to total protein in the lysates. For all graphs, data are from three independent differentiations, two wells per differentiation. Mean ± SEM, *p < 0.05, **p < 0.01, ns = no significance by one-way ANOVA and Dunnett's post test using WT as the control group.

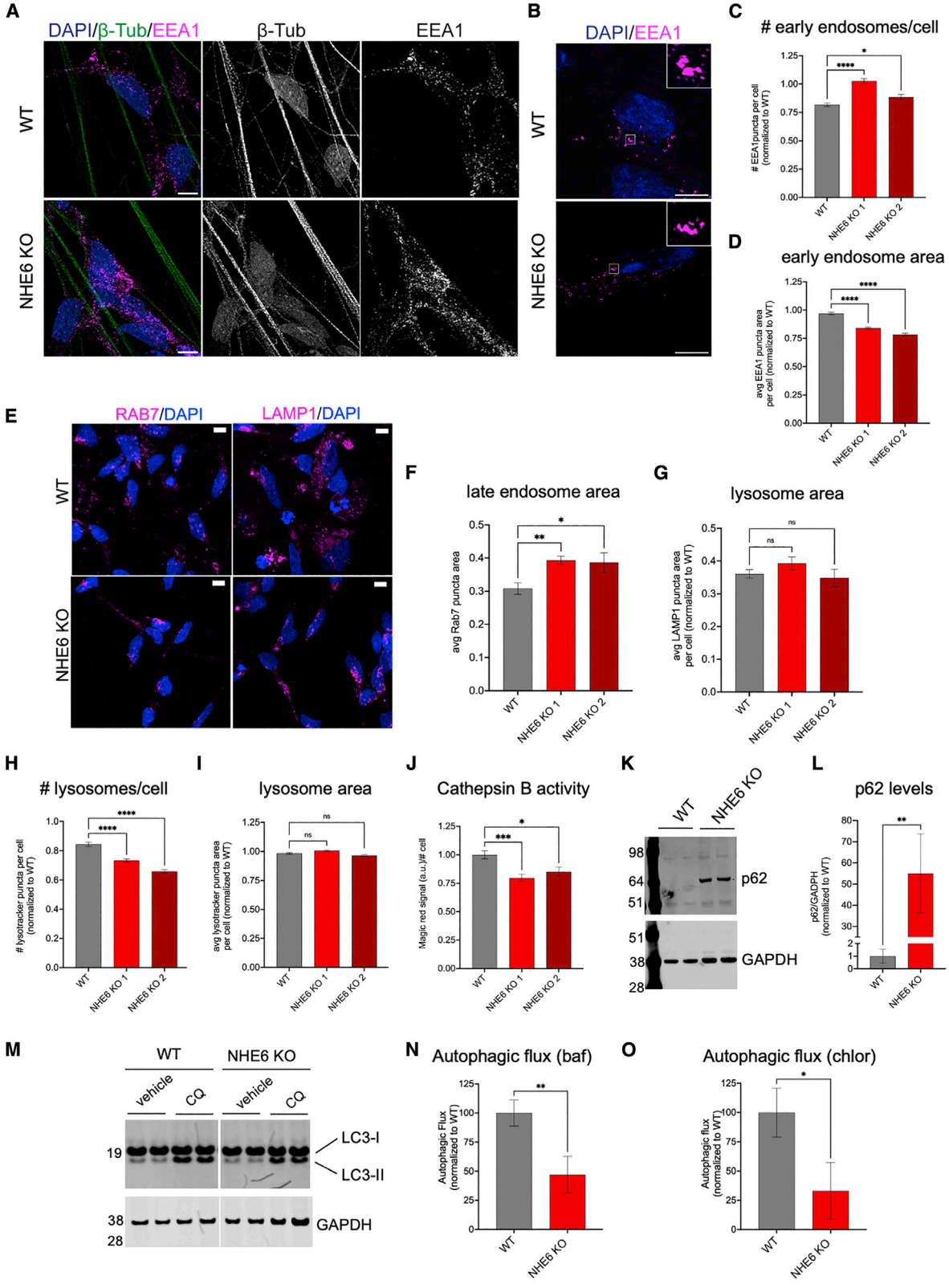

(legend on next page)

reduction in phospho-tau levels, but instead it led to a specific reduction of the *elevated* phospho-tau observed in NHE6 KO neurons. We also demonstrated that trehalose treatment resulted in an expected increase in levels of LC3-II (Figure 7C). We validated that this elevation in LC3-II levels observed with trehalose treatment is a result of enhanced autophagy (and not impaired degradation by the lysosome) by treating cells with either trehalose, chloroquine, or both trehalose and chloroquine, followed by WB to monitor LC3-II levels. As shown in Figure 7D, treatment with trehalose and chloroquine individually elevated LC3-II levels, while the combined treatment with both trehalose and chloroquine elevated LC3-II levels even further. These results indicate that trehalose indeed enhances autophagic flux in iNs. Previous studies have reported increased levels of nuclear transcription factor EB (TFEB) in cells treated with trehalose (Evans et al., 2018; Jeong et al., 2021; Rusmini et al., 2019; Wang et al., 2018); however, we did not find that trehalose led to a detectable increase in nuclear localization of TFEB in iNs, suggesting that its effects on the autophagy-lysosome system in iNs may be TFEB-independent (Figure S6). We also found that trehalose did not alter levels of secreted Aβs (Figures S7A–S7C), supporting the hypothesis that the decreased levels of phospho-tau observed are not due to altered Aβ levels. Trehalose also did not reduce levels of α-synuclein in these neurons (Figure S7D), again indicating that its effect was specific to the elevated phospho-tau phenotype we observed with NHE6 KO. To further validate these results indicating that enhancement of autophagy rescues the elevated phospho-tau phenotype in CS neurons, we treated cells with rapamycin as an additional method to induce autophagy. As shown in Figures 7E and 7F, treatment of NHE6-null iNs with rapamycin significantly reduced the ratio of p202,205 tau relative to total tau.

Our lab has previously described iNs generated from patient-derived iPSC lines harboring fAD-causing mutations in APP (Muratore et al., 2017). We previously reported an increase in the ratio of aggregation-prone Aβ42 relative to Aβ40 generated by these fAD iNs compared with a CRISPR-corrected isogenic WT control line; the fAD iNs also exhibit an elevation in the p202,205 tau to total tau ratio compared with the WT control iNs (Muratore et al., 2017). To further probe the specificity of the rescue of elevated phospho-tau that we observed in NHE6 neurons, we asked whether trehalose would correct the elevated phospho-tau phenotype that occurs in the fAD neurons as a result of APP mutation. As shown in Figures 7H and 7I, we observed the expected increase in the phospho-tau to total tau ratio in the fAD iNs compared with WT. However, despite the treatment eliciting an increase in LC3-II levels of equal magnitude as in NHE6 KO neurons (Figure 7J), the phospho-tau phenotype in fAD neurons was not rescued by trehalose. This suggests a mechanistic difference between phospho-tau elevation resulting from APP mutation and altered Aβ production versus that which results from loss of NHE6 activity.

DISCUSSION

CS, a rare X-linked neurodevelopmental disorder with autistic features, is caused by loss-of-function mutations in NHE6, a protein that is central to the proper functioning of the endolysosomal system through its critical regulation of luminal pH. Recently, neurodegenerative features of CS

Figure 6. NHE6 KO results in changes in the endolysosomal and autophagy-lysosomal systems

(A and B) Representative high-resolution images of endosomes in WT and NHE6 KO iNs. Images in (A) were acquired via confocal microscopy (scale bars, 10 μm) and images in (B) via super-resolution microscopy (scale bars, 5 μm).

(C and D) Endosomal numbers and area were analyzed by EEA1 and DAPI immunostaining of fixed neurons. Area was measured on a per-endosome basis. Images were captured using an IN Cell analyzer and quantified using Cell Profiler. Endosomal number per cell (C) and area per endosome (D) were quantified across three independent differentiations, with two wells per line per differentiation. Nine images were taken per well.

(E) Representative images of late endosomes (RAB7) and lysosomes (LAMP1). Scale bar, 5 μm.

(F and G) Quantification of RAB7+ area and LAMP1+ area per cell.

(H and I) Live day 21 neurons were stained with Lysotracker and NucBlue live cell stain and analyzed as in (C) and (D). Somally localized lysosomal number per cell (H) and area of each punctum (I) were quantified across three independent differentiations.

(J) Cathepsin B activity in live iNs was analyzed by measuring the fluorescence of Magic Red (ImmunoChemistry Technologies) substrate. Magic red signal was quantified across three independent differentiations using an Incucyte and normalized to cell body number quantified in each well by the Incucyte Neurotrack software.

(K) p62 levels in WT and NHE6 KO iNs were analyzed by WB of iN lysates.

(L) Quantification of p62 levels relative to GAPDH levels across three independent differentiations.

(M) Autophagic flux was quantified by treatment of iNs with bafilomycin A or chloroquine, followed by LC3 WB.

(N and O) Autophagic flux in WT and NHE6 KO neurons was calculated across three independent differentiations, with two wells per condition per differentiation. For all graphs, mean ± SEM is shown. *$p < 0.05$, **$p < 0.01$, ****$p < 0.0001$ one-way ANOVA and Dunnett's post test using WT as the control group. For (N) and (O), *$p < 0.05$, **$p < 0.01$ paired t test. For (L), **$p < 0.01$ unpaired t test.

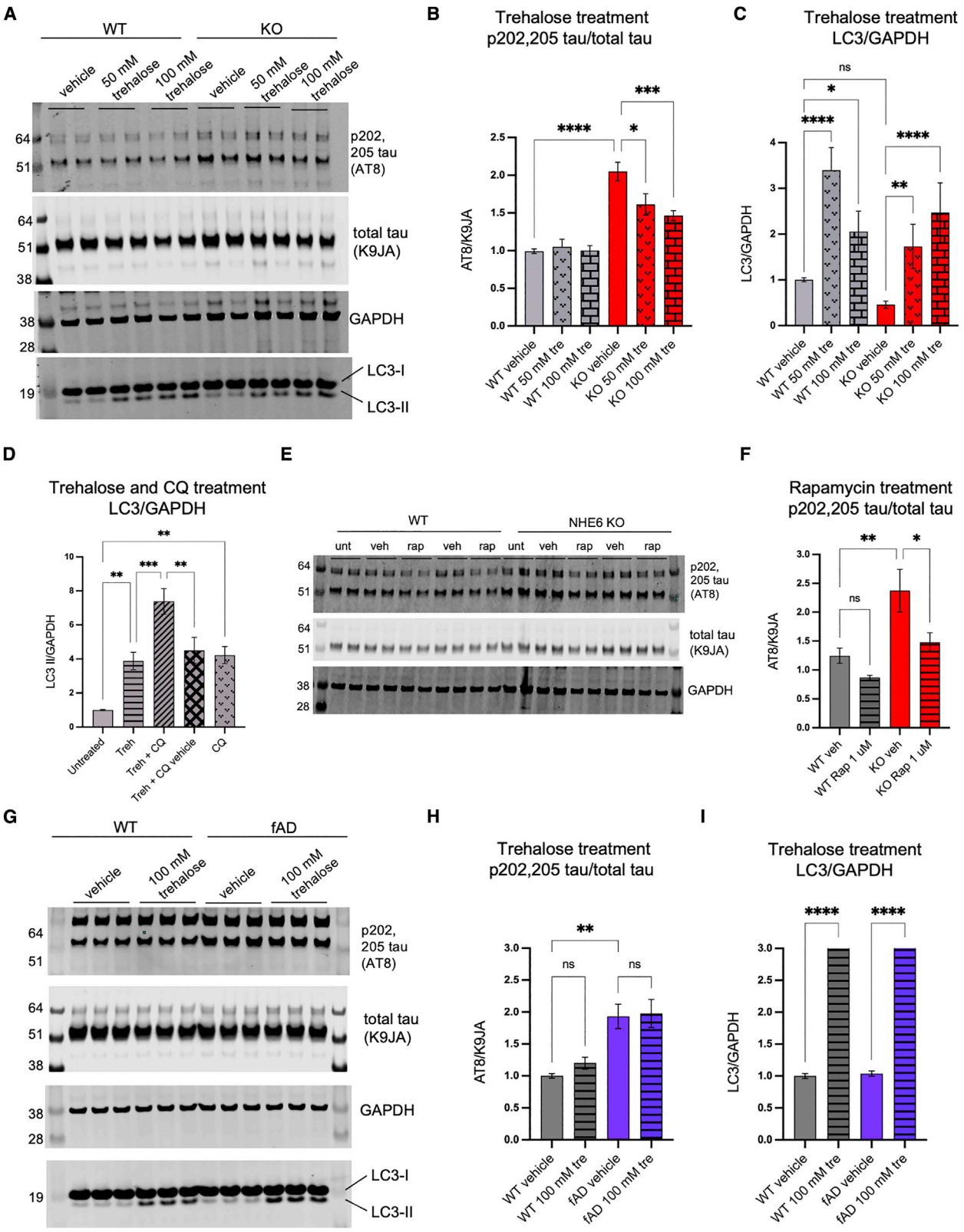

(legend on next page)

have become increasingly appreciated, with progressive neuronal loss observed in CS mice and rats along with evidence of tau deposition in CS patient brains (Garbern et al., 2010; Lee et al., 2021; Xu et al., 2017). Clinically, the severity of the syndrome in males makes neurodevelopmental and neurodegenerative symptoms difficult to parse; however, it has been reported that female carriers of CS mutations have been diagnosed with neurodegenerative clinical syndromes typically associated with tau deposition (Pescosolido et al., 2019). Intriguingly, analysis of gene expression data from deeply phenotyped ROS/MAP participants further connects NHE6 and tau pathology: decreased NHE6 expression in postmortem brains from this cohort correlates with increased levels of tau deposition. Moreover, NHE6 expression has been shown to be decreased in postmortem AD brains compared with age-matched controls (Prasad and Rao, 2015). Examining neurodegenerative features resulting from loss of NHE6 activity could have important implications for CS patients and female mutation carriers and, more broadly, could provide insight into the molecular underpinnings of tauopathies and the role of the endosome in neurodegeneration.

We differentiated isogenic NHE6 KO and WT human iPSC lines into iNs. The iN model used in this study is advantageous for several reasons. First, it allows for the generation of pure and highly consistent cortical neurons across differentiation rounds, providing an opportunity to interrogate neuronal phenotypes resulting from genetic or pharmacologic manipulation in a reductionist manner. In addition, bypassing the neuronal precursor stage via NGN2 expression reduced potentially confounding neurodevelopmental effects of NHE6 KO and allowed for more direct examination of neurodegenerative features. We and others have demonstrated the utility of using iNs to examine neurodegenerative changes in tau and other key proteins, as well as dysfunction of the endolysosomal system, in numerous disease models (D'Souza et al., 2021; Imberdis et al., 2019; Lagomarsino et al., 2021; Lin et al., 2018; Muratore et al., 2017; Sanyal et al., 2020).

Previous studies in NHE6-null mice and rats reported phenotypes indicating lysosomal defects in neurons (Lee et al., 2021; Pescosolido et al., 2021; Stromme et al., 2011). We also found evidence here that loss of this endosomal protein leads to subsequent lysosomal dysfunction in human neurons: NHE6 KO neurons in our study exhibited decreased numbers of soma-localized lysosomes per cell as well as decreased lysosomal protease activity. Lysosomal deficiency has been demonstrated to result in autophagy defects, as the cargo within autophagosomes is degraded upon fusion with the lysosome (Nixon, 2013; Schapansky et al., 2018; Wolfe et al., 2013). Aging NHE6-null rat brains displayed abnormal accumulation of autophagosomes and p62 aggregates (Lee et al., 2021). Therefore, we also examined NHE6 KO neurons for autophagy defects. Autophagic flux assays revealed a greater than 50% reduction in autophagic flux in NHE6 KO neurons compared with WT. We also observed pronounced accumulation of p62 in NHE6 KO iNs, while p62 was only present at low levels in WT iNs.

Importantly, we provide evidence that the elevated phospho-tau phenotype observed in NHE6 KO neurons is a result of the endolysosomal and autophagy-lysosomal dysfunction outlined above. Treatment of iNs with trehalose, which has been shown to enhance cellular clearance by autophagy and which resulted in the expected increase in autophagic flux in iNs, partially rescued the elevated phospho-tau phenotype in NHE6 KO iNs. Similarly, activation of autophagy with rapamycin treatment also rescued the phospho-tau levels. Intriguingly, we found that trehalose specifically reduces the elevation in phospho-tau caused by loss of NHE6 activity, as it did not alter phospho-tau levels in WT neurons, nor did it rescue elevated phospho-tau caused

Figure 7. Trehalose and rapamycin treatments partially rescue the elevated phosphorylated tau phenotype in NHE6 KO neurons

(A–D) iNs were treated with 50 mM or 100 mM trehalose starting from day 17 of differentiation.

(A) Cells were lysed on day 21, and levels of total tau and phosphorylated tau were examined by WB. Blots were probed for LC3 as a positive control for trehalose treatment, as trehalose has previously been shown to result in the observed increased in LC3-II (B and C). Quantification of WB data from three independent differentiations, with two wells per condition per differentiation.

(D) Quantification of LC3-II levels in cells treated with trehalose, chloroquine, or both trehalose and chloroquine were monitored by WB across three independent differentiations.

(E and F) iNs were treated with rapamycin starting from day 17 of differentiation. Cells were lysed on day 21, and levels of total and phosphorylated tau were examined as in (A).

(F) Quantification of WB data from three independent differentiations, with 2–4 wells per condition per differentiation.

(G–I) iNs harboring the fAD-causing London mutation in APP and a WT isogenic control line were treated with 100 mM trehalose starting from day 17 of differentiation as in (A). Cells were lysed on day 21 and levels of total tau, phosphorylated tau, and LC3 were examined by WB.

(H and I) Quantification of WB data from three independent differentiations, with three wells per condition per differentiation. While the fAD line displayed elevated p202,205 tau compared with WT, trehalose did not rescue this phenotype. For all graphs, mean ± SEM, *p < 0.05, **p < 0.01, ***p < 0.005, ****p < 0.0001 by one-way ANOVA and Sidak's post test.

by an fAD mutation in APP. The latter result suggests that, in iNs, the effects of APP mutation and resultant altered Aβ production are mechanistically distinct from the impacts of NHE6 KO on tau biology. In particular, altered tau kinase or phosphatase activity described in AD iPSC-derived neurons (Israel et al., 2012; Ochalek et al., 2017) would perhaps be unresponsive to trehalose treatment, while the autophagy-lysosomal defects resulting from NHE6 loss of function are mechanistically linked to the action of trehalose and would therefore allow for the specific rescue of tau phenotypes in these neurons.

Recent studies have linked NHE6 function in regulating endosomal pH with APOE4-induced defects in endolysosomal trafficking in neurons (Pohlkamp et al., 2021; Xian et al., 2018). These studies have led to the proposal that enhancement of acidification of endosomes via inhibition of NHE6 actually may be beneficial to reduce the negative consequences of APOE4 on trafficking and amyloid plaque deposition. Taken together with the data here, these results suggest that the fine-tuning of NHE6 activity is critical for maintaining endolysosomal function in neurons.

Our study provides important information about the role of NHE6 loss of function in neurodegeneration in human cortical neurons. The impact of NHE6 activity on neurodegenerative processes underlies the importance of future study of NHE6 loss of function in female neurons, which would encompass the added complexity of X chromosome inactivation and resulting mosaicism. In addition, myriad powerful protocols have been developed in recent years for the differentiation of numerous cell types of the CNS. Future work could expand on our current study and examine the effects of NHE6 loss of function in other neuronal subtypes, in astrocytes and microglia, and in mixed cultures of these cells. In particular, a pronounced glial response has been reported in NHE6 KO mice and rats (Lee et al., 2021; Pohlkamp et al., 2021; Xu et al., 2017) and in CS patient brain tissue (Garbern et al., 2010). Therefore, future study of glial activation and dysfunction in the context of NHE6 loss of function will be crucial for a fuller understanding of neurodegeneration in NHE6-null brains.

EXPERIMENTAL PROCEDURES

Induced pluripotent stem cell lines and culture

The Institutional Review Boards at Brown University and Lifespan Healthcare approved the human subjects research protocol. Informed consent was obtained from all participants or guardians of participants. The generation and characterization of the isogenic WT and CRISPR KO iPSC lines, as well as the patient-derived CS NHE6 mutant and CRISPR-corrected WT isogenic control iPSC lines, has been previously described (Lizarraga et al., 2021; Ma et al., 2021). iPSCs were plated on Matrigel (Corning). Cultures were maintained in Stemflex media (Thermo Fisher Scientific) and continually monitored for quality.

Induced neuron differentiations

iN differentiations were carried out via the expression of Neurogenin-2 (NGN2) as previously described (Srikanth et al., 2018; Zhang et al., 2013). iPSC lines were co-transduced with lentiviruses containing pTet-*O*-Ngn2-puro and FudeltaGW-rtTA, which are constructs that allow for the dox-inducible expression of NGN2. The puromycin resistance cassette allows for the selection of cells expressing NGN2. Transduced cells were expanded and plated in 10-cm dishes in Stemflex media. The next day (day 1), cells were fed with KSR media with doxycycline (2 μg/mL, Sigma) to induce NGN2 expression. On day 2, cells were fed with 1:1 KSR:N2B media with doxycycline and puromycin (10 μg/mL, Gibco). The next day, cells were fed with N2B media supplemented with 1:100 B27 (Life Technologies), doxycycline, and puromycin. On day 4, cells were dissociated with Accutase and banked as frozen stocks. Day 4 cells were then plated on tissue culture plates coated with poly-L-orthinine and laminin followed by Matrigel. iNs were plated in Neurobasal media supplemented with B27, doxycycline, and puromycin and maintained with half media changes of this media until they were harvested. Where indicated, cells were cultured from day 4 on with the addition of 10 ng/mL BDNF, GDNF, and CNTF (Peprotech).

Statistical analysis

Data were analyzed using GraphPad Prism 9. Data are shown as mean ± SEM. Statistical significance between more than two groups was tested by one-way ANOVA followed by either Sidak's or Dunnet's post test as indicated. Comparisons between two groups were carried out by either an unpaired Student's t test or a paired Student's t test, as indicated.

SUPPLEMENTAL INFORMATION

Supplemental information, including additional details regarding experimental procedures, can be found online at https://doi.org/10.1016/j.stemcr.2022.08.001.

AUTHOR CONTRIBUTIONS

M.A.F., T.Y.P., and E.M.M. designed experiments and analyzed data. M.F., F.B., E.W., and Y.L. conducted experiments. M.F. and T.Y.P. wrote the manuscript. L.M. and M.S. generated and characterized the iPSC lines used in this study. E.M.M. edited the manuscript. All authors read and approved the final manuscript.

ACKNOWLEDGMENTS

We thank Dennis Selkoe and members of the Young-Pearse lab for helpful discussions. This work was supported by NIH grants: R01NS113141 (E.M.M.), R01AG055909 (T.Y.P), R01NS117446 (T.Y.P), and K22NS107802 (M.A.F.).

CONFLICTS OF INTEREST

The authors declare no competing interests.

Received: January 17, 2022
Revised: August 3, 2022
Accepted: August 3, 2022
Published: September 1, 2022

REFERENCES

Belzile, J.P., Sabalza, M., Craig, M., Clark, A.E., Morello, C.S., and Spector, D.H. (2016). Trehalose, an mTOR-independent inducer of autophagy, inhibits human cytomegalovirus infection in multiple cell types. J. Virol. *90*, 1259–1277.

Biernat, J., Mandelkow, E.M., Schröter, C., Lichtenberg-Kraag, B., Steiner, B., Berling, B., Meyer, H., Mercken, M., Vandermeeren, A., Goedert, M., et al. (1992). The switch of tau protein to an Alzheimer-like state includes the phosphorylation of two serine-proline motifs upstream of the microtubule binding region. EMBO J. *11*, 1593–1597.

Borden, L.A., Einstein, R., Gabel, C.A., and Maxfield, F.R. (1990). Acidification-dependent dissociation of endocytosed insulin precedes that of endocytosed proteins bearing the mannose 6-phosphate recognition marker. J. Biol. Chem. *265*, 8497–8504.

Braak, E., Braak, H., and Mandelkow, E.M. (1994). A sequence of cytoskeleton changes related to the formation of neurofibrillary tangles and neuropil threads. Acta Neuropathol. *87*, 554–567.

Casarejos, M.J., Solano, R.M., Gómez, A., Perucho, J., de Yébenes, J.G., and Mena, M.A. (2011). The accumulation of neurotoxic proteins, induced by proteasome inhibition, is reverted by trehalose, an enhancer of autophagy, in human neuroblastoma cells. Neurochem. Int. *58*, 512–520.

Casey, J.R., Grinstein, S., and Orlowski, J. (2010). Sensors and regulators of intracellular pH. Nat. Rev. Mol. Cell Biol. *11*, 50–61.

Castillo, K., Nassif, M., Valenzuela, V., Rojas, F., Matus, S., Mercado, G., Court, F.A., van Zundert, B., and Hetz, C. (2013). Trehalose delays the progression of amyotrophic lateral sclerosis by enhancing autophagy in motoneurons. Autophagy *9*, 1308–1320.

Christianson, A.L., Stevenson, R.E., van der Meyden, C.H., Pelser, J., Theron, F.W., van Rensburg, P.L., Chandler, M., and Schwartz, C.E. (1999). X linked severe mental retardation, craniofacial dysmorphology, epilepsy, ophthalmoplegia, and cerebellar atrophy in a large South African kindred is localised to Xq24-q27. J. Med. Genet. *36*, 759–766.

Colacurcio, D.J., Pensalfini, A., Jiang, Y., and Nixon, R.A. (2018). Dysfunction of autophagy and endosomal-lysosomal pathways: roles in pathogenesis of Down syndrome and Alzheimer's Disease. Free Radic. Biol. Med. *114*, 40–51.

D'Souza, G.X., Rose, S.E., Knupp, A., Nicholson, D.A., Keene, C.D., and Young, J.E. (2021). The application of in vitro-derived human neurons in neurodegenerative disease modeling. J. Neurosci. Res. *99*, 124–140.

Das, U., Scott, D.A., Ganguly, A., Koo, E.H., Tang, Y., and Roy, S. (2013). Activity-induced convergence of APP and BACE-1 in acidic microdomains via an endocytosis-dependent pathway. Neuron *79*, 447–460.

Dautry-Varsat, A., Ciechanover, A., and Lodish, H.F. (1983). pH and the recycling of transferrin during receptor-mediated endocytosis. Proc. Natl. Acad. Sci. USA *80*, 2258–2262.

De Strooper, B., Iwatsubo, T., and Wolfe, M.S. (2012). Presenilins and gamma-secretase: structure, function, and role in Alzheimer Disease. Cold Spring Harb. Perspect. Med. *2*, a006304.

Diering, G.H., and Numata, M. (2014). Endosomal pH in neuronal signaling and synaptic transmission: role of Na(+)/H(+) exchanger NHE5. Front. Physiol. *4*, 412.

Donowitz, M., Ming Tse, C., and Fuster, D. (2013). SLC9/NHE gene family, a plasma membrane and organellar family of Na(+)/H(+) exchangers. Mol. Aspects Med. *34*, 236–251.

Esler, W.P., and Wolfe, M.S. (2001). A portrait of Alzheimer secretases–new features and familiar faces. Science *293*, 1449–1454.

Evans, T.D., Jeong, S.J., Zhang, X., Sergin, I., and Razani, B. (2018). TFEB and trehalose drive the macrophage autophagy-lysosome system to protect against atherosclerosis. Autophagy *14*, 724–726.

Garbern, J.Y., Neumann, M., Trojanowski, J.Q., Lee, V.M.Y., Feldman, G., Norris, J.W., Friez, M.J., Schwartz, C.E., Stevenson, R., and Sima, A.A.F. (2010). A mutation affecting the sodium/proton exchanger, SLC9A6, causes mental retardation with tau deposition. Brain *133*, 1391–1402.

Gilfillan, G.D., Selmer, K.K., Roxrud, I., Smith, R., Kyllerman, M., Eiklid, K., Kroken, M., Mattingsdal, M., Egeland, T., Stenmark, H., et al. (2008). SLC9A6 mutations cause X-linked mental retardation, microcephaly, epilepsy, and ataxia, a phenotype mimicking Angelman syndrome. Am. J. Hum. Genet. *82*, 1003–1010.

Giovedi, S., Ravanelli, M.M., Parisi, B., Bettegazzi, B., and Guarnieri, F.C. (2020). Dysfunctional autophagy and endolysosomal system in neurodegenerative diseases: relevance and therapeutic options. Front. Cell. Neurosci. *14*, 602116.

Haass, C., and Selkoe, D.J. (1993). Cellular processing of beta-amyloid precursor protein and the genesis of amyloid beta-peptide. Cell *75*, 1039–1042.

Hampel, H., Vassar, R., De Strooper, B., Hardy, J., Willem, M., Singh, N., Zhou, J., Yan, R., Vanmechelen, E., De Vos, A., et al. (2021). The beta-Secretase BACE1 in Alzheimer's Disease. Biol. Psychiatr. *89*, 745–756.

Imberdis, T., Negri, J., Ramalingam, N., Terry-Kantor, E., Ho, G.P.H., Fanning, S., Stirtz, G., Kim, T.E., Levy, O.A., Young-Pearse, T.L., et al. (2019). Cell models of lipid-rich alpha-synuclein aggregation validate known modifiers of alpha-synuclein biology and identify stearoyl-CoA desaturase. Proc. Natl. Acad. Sci. USA *116*, 20760–20769.

Israel, M.A., Yuan, S.H., Bardy, C., Reyna, S.M., Mu, Y., Herrera, C., Hefferan, M.P., Van Gorp, S., Nazor, K.L., Boscolo, F.S., et al. (2012). Probing sporadic and familial Alzheimer's disease using induced pluripotent stem cells. Nature *482*, 216–220.

Jeong, S.J., Stitham, J., Evans, T.D., Zhang, X., Rodriguez-Velez, A., Yeh, Y.S., Tao, J., Takabatake, K., Epelman, S., Lodhi, I.J., et al. (2021). Trehalose causes low-grade lysosomal stress to activate TFEB and the autophagy-lysosome biogenesis response. Autophagy *17*, 3740–3752.

Klionsky, D.J., Abdelmohsen, K., Abe, A., Abedin, M.J., Abeliovich, H., Acevedo Arozena, A., Adachi, H., Adams, C.M., Adams, P.D.,

Adeli, K., et al. (2016). Guidelines for the use and interpretation of assays for monitoring autophagy. Autophagy *12*, 1–382. 3rd edition.

Kondapalli, K.C., Prasad, H., and Rao, R. (2014). An inside job: how endosomal Na(+)/H(+) exchangers link to autism and neurological disease. Front. Cell. Neurosci. *8*, 172.

Kruger, U., Wang, Y., Kumar, S., and Mandelkow, E.M. (2012). Autophagic degradation of tau in primary neurons and its enhancement by trehalose. Neurobiol. Aging *33*, 2291–2305.

Lagomarsino, V.N., Pearse, R.V., 2nd, Liu, L., Hsieh, Y.C., Fernandez, M.A., Vinton, E.A., Paull, D., Felsky, D., Tasaki, S., Gaiteri, C., et al. (2021). Stem cell-derived neurons reflect features of protein networks, neuropathology, and cognitive outcome of their aged human donors. Neuron *109*, 3402–3420.e9.

Lee, Y., Miller, M.R., Fernandez, M.A., Berg, E.L., Prada, A.M., Ouyang, Q., Schmidt, M., Silverman, J.L., Young-Pearse, T.L., and Morrow, E.M. (2021). Early lysosome defects precede neurodegeneration with amyloid-beta and tau aggregation in NHE6-null rat brain. Brain, awab467.

Lin, Y.T., Seo, J., Gao, F., Feldman, H.M., Wen, H.L., Penney, J., Cam, H.P., Gjoneska, E., Raja, W.K., Cheng, J., et al. (2018). APOE4 causes widespread molecular and cellular alterations associated with Alzheimer's disease phenotypes in human iPSC-derived brain cell types. Neuron *98*, 1294.

Lizarraga, S.B., Ma, L., Maguire, A.M., van Dyck, L.I., Wu, Q., Ouyang, Q., Kavanaugh, B.C., Nagda, D., Livi, L.L., Pescosolido, M.F., et al. (2021). Human neurons from Christianson syndrome iPSCs reveal mutation-specific responses to rescue strategies. Sci. Transl. Med. *13*, eaaw0682.

Ma, L., Schmidt, M., and Morrow, E.M. (2021). Human iPSC lines from a Christianson syndrome patient with NHE6 W523X mutation, a biologically-related control, and CRISPR/Cas9 gene-corrected isogenic controls. Stem Cell Res. *54*, 102435.

Malik, B.R., Maddison, D.C., Smith, G.A., and Peters, O.M. (2019). Autophagic and endo-lysosomal dysfunction in neurodegenerative disease. Mol. Brain *12*, 100.

Mellman, I. (1992). The importance of being acid: the role of acidification in intracellular membrane traffic. J. Exp. Biol. *172*, 39–45.

Muratore, C.R., Rice, H.C., Srikanth, P., Callahan, D.G., Shin, T., Benjamin, L.N.P., Walsh, D.M., Selkoe, D.J., and Young-Pearse, T.L. (2014). The familial Alzheimer's disease APPV717I mutation alters APP processing and Tau expression in iPSC-derived neurons. Hum. Mol. Genet. *23*, 3523–3536.

Muratore, C.R., Zhou, C., Liao, M., Fernandez, M.A., Taylor, W.M., Lagomarsino, V.N., Pearse, R.V., 2nd, Rice, H.C., Negri, J.M., He, A., et al. (2017). Cell-type dependent Alzheimer's disease phenotypes: probing the biology of selective neuronal vulnerability. Stem Cell Rep. *9*, 1868–1884.

Nixon, R.A. (2013). The role of autophagy in neurodegenerative disease. Nat. Med. *19*, 983–997.

Nixon, R.A., Yang, D.S., and Lee, J.H. (2008). Neurodegenerative lysosomal disorders: a continuum from development to late age. Autophagy *4*, 590–599.

Ochalek, A., Mihalik, B., Avci, H.X., Chandrasekaran, A., Téglási, A., Bock, I., Giudice, M.L., Táncos, Z., Molnár, K., László, L., et al. (2017). Neurons derived from sporadic Alzheimer's disease iPSCs reveal elevated TAU hyperphosphorylation, increased amyloid levels, and GSK3B activation. Alzheimer's Res. Ther. *9*, 90.

Ouyang, Q., Lizarraga, S.B., Schmidt, M., Yang, U., Gong, J., Ellisor, D., Kauer, J.A., and Morrow, E.M. (2013). Christianson syndrome protein NHE6 modulates TrkB endosomal signaling required for neuronal circuit development. Neuron *80*, 97–112.

Parenti, G., Medina, D.L., and Ballabio, A. (2021). The rapidly evolving view of lysosomal storage diseases. EMBO Mol. Med. *13*, e12836.

Pescosolido, M.F., Kavanaugh, B.C., Pochet, N., Schmidt, M., Jerskey, B.A., Rogg, J.M., De Jager, P.L., Young-Pearse, T.L., Liu, J.S., and Morrow, E.M. (2019). Complex neurological phenotype in female carriers of NHE6 mutations. Mol. Neuropsychiatry *5*, 98–108.

Pescosolido, M.F., Ouyang, Q., Liu, J.S., and Morrow, E.M. (2021). Loss of Christianson syndrome Na(+)/H(+) exchanger 6 (NHE6) causes abnormal endosome maturation and trafficking underlying lysosome dysfunction in neurons. J. Neurosci. *41*, 9235–9256.

Pescosolido, M.F., Stein, D.M., Schmidt, M., El Achkar, C.M., Sabbagh, M., Rogg, J.M., Tantravahi, U., McLean, R.L., Liu, J.S., Poduri, A., et al. (2014). Genetic and phenotypic diversity of NHE6 mutations in Christianson syndrome. Ann. Neurol. *76*, 581–593.

Pillay, C.S., Elliott, E., and Dennison, C. (2002). Endolysosomal proteolysis and its regulation. Biochem. J. *363*, 417–429.

Pohlkamp, T., Xian, X., Wong, C.H., Durakoglugil, M.S., Werthmann, G.C., Saido, T.C., Evers, B.M., White, C.L., 3rd, Connor, J., Hammer, R.E., et al. (2021). NHE6 depletion corrects ApoE4-mediated synaptic impairments and reduces amyloid plaque load. Elife *10*, e72034.

Prasad, H., and Rao, R. (2015). The Na+/H+ exchanger NHE6 modulates endosomal pH to control processing of amyloid precursor protein in a cell culture model of Alzheimer disease. J. Biol. Chem. *290*, 5311–5327.

Rodríguez-Navarro, J.A., Rodríguez, L., Casarejos, M.J., Solano, R.M., Gómez, A., Perucho, J., Cuervo, A.M., García de Yébenes, J., and Mena, M.A. (2010). Trehalose ameliorates dopaminergic and tau pathology in parkin deleted/tau overexpressing mice through autophagy activation. Neurobiol. Dis. *39*, 423–438.

Rusmini, P., Cortese, K., Crippa, V., Cristofani, R., Cicardi, M.E., Ferrari, V., Vezzoli, G., Tedesco, B., Meroni, M., Messi, E., et al. (2019). Trehalose induces autophagy via lysosomal-mediated TFEB activation in models of motoneuron degeneration. Autophagy *15*, 631–651.

Sannerud, R., Declerck, I., Peric, A., Raemaekers, T., Menendez, G., Zhou, L., Veerle, B., Coen, K., Munck, S., De Strooper, B., et al. (2011). ADP ribosylation factor 6 (ARF6) controls amyloid precursor protein (APP) processing by mediating the endosomal sorting of BACE1. Proc. Natl. Acad. Sci. USA *108*, E559–E568.

Sanyal, A., Novis, H.S., Gasser, E., Lin, S., and LaVoie, M.J. (2020). LRRK2 kinase inhibition rescues deficits in lysosome function due to heterozygous GBA1 expression in human iPSC-derived neurons. Front. Neurosci. *14*, 442.

Sarkar, S., Davies, J.E., Huang, Z., Tunnacliffe, A., and Rubinsztein, D.C. (2007). Trehalose, a novel mTOR-independent autophagy

enhancer, accelerates the clearance of mutant huntingtin and alpha-synuclein. J. Biol. Chem. *282*, 5641–5652.

Schapansky, J., Khasnavis, S., DeAndrade, M.P., Nardozzi, J.D., Falkson, S.R., Boyd, J.D., Sanderson, J.B., Bartels, T., Melrose, H.L., and LaVoie, M.J. (2018). Familial knockin mutation of LRRK2 causes lysosomal dysfunction and accumulation of endogenous insoluble alpha-synuclein in neurons. Neurobiol. Dis. *111*, 26–35.

Schneider, A., Rajendran, L., Honsho, M., Gralle, M., Donnert, G., Wouters, F., Hell, S.W., and Simons, M. (2008). Flotillin-dependent clustering of the amyloid precursor protein regulates its endocytosis and amyloidogenic processing in neurons. J. Neurosci. *28*, 2874–2882.

Sikora, J., Leddy, J., Gulinello, M., and Walkley, S.U. (2016). X-linked Christianson syndrome: heterozygous female Slc9a6 knockout mice develop mosaic neuropathological changes and related behavioral abnormalities. Dis. Model. Mech. *9*, 13–23.

Sinajon, P., Verbaan, D., and So, J. (2016). The expanding phenotypic spectrum of female SLC9A6 mutation carriers: a case series and review of the literature. Hum. Genet. *135*, 841–850.

Srikanth, P., Lagomarsino, V.N., Pearse, R.V., 2nd, Liao, M., Ghosh, S., Nehme, R., Seyfried, N., Eggan, K., and Young-Pearse, T.L. (2018). Convergence of independent DISC1 mutations on impaired neurite growth via decreased UNC5D expression. Transl. Psychiatry *8*, 245.

Stromme, P., Dobrenis, K., Sillitoe, R.V., Gulinello, M., Ali, N.F., Davidson, C., Micsenyi, M.C., Stephney, G., Ellevog, L., Klungland, A., et al. (2011). X-linked Angelman-like syndrome caused by Slc9a6 knockout in mice exhibits evidence of endosomal-lysosomal dysfunction. Brain *134*, 3369–3383.

Van Acker, Z.P., Bretou, M., and Annaert, W. (2019). Endo-lysosomal dysregulations and late-onset Alzheimer's disease: impact of genetic risk factors. Mol. Neurodegener. *14*, 20.

Vassar, R., Kovacs, D.M., Yan, R., and Wong, P.C. (2009). The beta-secretase enzyme BACE in health and Alzheimer's disease: regulation, cell biology, function, and therapeutic potential. J. Neurosci. *29*, 12787–12794.

Wang, Y., Liu, F.T., Wang, Y.X., Guan, R.Y., Chen, C., Li, D.K., Bu, L.L., Song, J., Yang, Y.J., Dong, Y., et al. (2018). Autophagic modulation by trehalose reduces accumulation of TDP-43 in a cell model of amyotrophic lateral sclerosis via TFEB activation. Neurotox. Res. *34*, 109–120.

Wolfe, D.M., Lee, J.H., Kumar, A., Lee, S., Orenstein, S.J., and Nixon, R.A. (2013). Autophagy failure in Alzheimer's disease and the role of defective lysosomal acidification. Eur. J. Neurosci. *37*, 1949–1961.

Xian, X., Pohlkamp, T., Durakoglugil, M.S., Wong, C.H., Beck, J.K., Lane-Donovan, C., Plattner, F., and Herz, J. (2018). Reversal of ApoE4-induced recycling block as a novel prevention approach for Alzheimer's disease. Elife *7*, e40048.

Xu, M., Ouyang, Q., Gong, J., Pescosolido, M.F., Pruett, B.S., Mishra, S., Schmidt, M., Jones, R.N., Gamsiz Uzun, E.D., Lizarraga, S.B., et al. (2017). Mixed neurodevelopmental and neurodegenerative pathology in Nhe6-null mouse model of Christianson syndrome. eNeuro *4*. ENEURO.0388-17.2017.

Yamashiro, D.J., and Maxfield, F.R. (1984). Acidification of endocytic compartments and the intracellular pathways of ligands and receptors. J. Cell. Biochem. *26*, 231–246.

Zhang, X., Chen, S., Song, L., Tang, Y., Shen, Y., Jia, L., and Le, W. (2014). MTOR-independent, autophagic enhancer trehalose prolongs motor neuron survival and ameliorates the autophagic flux defect in a mouse model of amyotrophic lateral sclerosis. Autophagy *10*, 588–602.

Zhang, Y., Pak, C., Han, Y., Ahlenius, H., Zhang, Z., Chanda, S., Marro, S., Patzke, C., Acuna, C., Covy, J., et al. (2013). Rapid single-step induction of functional neurons from human pluripotent stem cells. Neuron *78*, 785–798.